Aerosol and Air Quality Research, 16: 301–313, 2016

ISSN: 1680-8584 print / 2071-1409 online
doi: 10.4209/aaqr.2015.03.0191

Evaporation and Movement of Fine Water Droplets Influenced by Initial Diameter and Relative Humidity

Yi Wang[1*], Yang Yang[1], Yan Zou[1], Yingxue Cao[1], Xiaofen Ren[2], Yanbin Li[1]

[1] *Xi'an University of Architecture and Technology, Xi'an, 710055, China*
[2] *Heibei University of Engineering, Hebei, 056038, China*

ABSTRACT

Droplets generated in industrial buildings may do harm to the workers, the construction and the environment. Ventilation is often used to control this kind of air-borne contaminants. In order to provide a basis and reference for the efficient ventilation on droplets control, a numerical simulation method is adopted to reveal the evaporation and movement of fine water droplet populations released from a tank in industrial buildings. The variations of diameter and velocity of water droplets with identical initial diameter and velocity were studied. The results showed the evaporation and movement of the droplet populations presented obviously nonuniform distributions, due to vapor concentration and velocity distribution of the air around the droplets. When the droplets were closer to the centerline of the tank, they showed a lower evaporation rate, a larger velocity and a bigger velocity difference between droplets and its surrounding air. The effects of initial diameter and the relative humidity of the ambient air on droplet evaporation and movement were discussed. Compared to the relative humidity of the ambient air, the initial diameter had a more significant effect on the droplet evaporation and movement. The effects of the initial diameter variation (1 μm–50 μm) on the evaporation time variation and the terminal height variation were almost 17 times and 10 times larger than the effects by the relative humidity variation of the ambient air (20%–80%), respectively.

Keywords: Aerosol; Droplet evaporation; Droplet movement; Numerical simulation; Lagrangian-Eulerian approach.

INTRODUCTION

Water or acidic droplets are substantially generated in many production processes in industrial buildings, such as water cooling, electrolysis, and pickling. After the droplets escape into the operating environment, they may endanger the health of industrial workers (Hyunhee, 2013; Li and Zhou, 2015). The high humidity or acidic environments created by the droplets may cause equipment corrosion, construction damage, structural heat transfer coefficient increasement, etc. (Achenbach and Trechsel, 1982). Meanwhile, the mist generated by droplets may impede normal production and worker operations.

Ventilation, using airflow to transport and capture air-borne contaminants, is a common and useful control method. However, the current ventilation design handbooks on droplet control do not take the characteristics of the droplet movement into consideration (Sun, 1997; ASHRAE, 2007). Revealing the movement of droplets in air could contribute to finding a reasonable and effective ventilation control method, which plays an important role in protecting workers' health, prolonging the life of equipment and buildings, and ensuring normal production and operating conditions.

The movement of droplets is different from that of gas contaminants and solid particles because evaporation causes the forces acting on the droplets to change constantly; therefore, evaporation and these forces should be well understood. Many evaporation models are proposed based on different assumptions and influencing factors. They are mainly divided into the infinite thermal conductivity model (Sazhin, 2006), the finite thermal conductivity model (Miller *et al.*, 1998) and the vortex model (Sirignano, 2000), according to the assumption of droplet temperature uniformity. Droplet size is usually small (less than 1000 μm) in an indoor air environment, and the infinite thermal conductivity model is typically used to describe the evaporation of these tiny droplets. The evaporation prediction suitable for fine droplets was further developed by Kukkonen (1989) who considered Stefan flow and the temperature dependence of the diffusion coefficient to improve a widely adopted model to predict the evaporation. When a droplet is a solution such as an acid or salt solution, the evaporation rate of the droplet is affected because of the solute to water effect (Dufour and Defay, 1963; Pruppacher and Klett, 2004). Zhao *et al*. (2004)

* Corresponding author.
Tel.: 86 029 82202729; Fax: 0086 029 82202729
E-mail address: wangyi6920@126.com

found that the pressure gradient force, visual mass force and the Basset force could be negligible. The drag force acting on a droplet can be described by the Stokes correction form considering the slip effect and the Reynolds number (Allen and Raabe, 1982).These studies deepened the understanding of the movement of fine droplets in an indoor air environment.

With the development of the computer, numerical simulation technology has become an important means of studying the evaporation and motion characteristics of droplets (Varghese and Gangamma, 2007; Xie *et al.*, 2007; Shanthanu *et al.*, 2013; Zhou *et al.*, 2013). The evaporation of droplets with solid particles was researched based on a numerical simulation; and the process could be divided into two stages with the former stage being similar to pure water droplet evaporation (Cheong, 1986; Kadja and Bergeles, 2003). The motion characteristic of evaporating droplets in a three-dimensional incompressible fluid was presented, based on the volume-of-fluid (VOF) multiphase flow approach with direct numerical simulation (Schlottkea and Weigand, 2008). Furthermore, numerical simulation technology is also adopted to study the evaporation and motion of droplets in different practical engineering situations. The effects of the channel geometry on the droplet dynamics in fuel cells had been numerically investigated (Zhu *et al.*, 2010; Kim *et al.*, 2014). Montazeri *et al.* (2015a) found that a numerical simulation by a Lagrangian-Eulerian approach could accurately predict droplet evaporation in evaporative cooling by water spray systems in outdoor and indoor urban environments, and the impact of physical parameters on evaporative cooling by a mist spray system were researched with CFD analysis (Montazeri *et al.*, 2015b). A Lagrangian-Eulerian approach was employed to research the motion of evaporating droplets exhaled by human beings in a ventilated room, and the results were intended to provide effective measures to reduce the infection risk of others by droplets exhaled by patients (Sun and Ji, 2007; Liu, 2011).

Obviously, plenty of researches have been completed to examine the evaporation and movement of droplets. For droplets in industrial buildings, however, their evaporation and motion are more influenced by nonuniform relative humidity, velocity and temperature distribution of air and other environmental parameters that are related to production processes. Meanwhile, the droplet composition, initial diameter and flow mode in this environment are also different from those in existing studies. It is very important to reveal the movement of evaporating droplets in typical production processes.

This paper focuses on the evaporation and movement of fine water droplet populations in nonuniform relative humidity, velocity distribution of indoor air. The droplets and the nonuniform environment are generated by a water cooling tank. Both the diameter evolution and velocity distribution of droplets were analysed when the initial droplet diameters and the relative humidity of the ambient air changed. The results are intended to provide a reference for reasonable and efficient ventilation methods of droplet control.

METHODOLOGY

A Lagrangian-Eulerian approach was employed to investigate the evaporation and movement of water droplets populations generated from a tank, based on numerical simulation.

Geometry, Boundary Conditions and Grid

The geometric model used in this paper is one part of a industrial building and shown in Fig. 1(a) and the size of the computational domain is 10 m × 10 m × 10 m. Actually, the space of the industrial buildings are usually very large, the air from other parts of the industrial building (i.e., the ambient air), could have an effect on the computational domain. In order to research the evaporation and movement difference of the droplets in the dry and wet the ambient air, both sides along the X-axis are set as pressure outlet boundary conditions and the air from the pressure outlet boundaries presents the ambient air. Thus the relative humidity of the ambient air (ARH) is presented by the relative humidity of air from pressure outlet boundaries. The other two sides along the Y-axis are the adiabatic wall boundary conditions. The top and bottom are the adiabatic wall boundary conditions. A tank in the bottom center of the room has a rectangular opening. The opening size is 1 m × 1 m, and the distance between the opening and the ground is 1 m. The tank opening is assumed to be the source surface releasing the pure water droplets and saturated moist air, and the reason for this assumption is mentioned in the Section *Airflow and droplet.* The coordinate origin, O, is at the midpoint of the tank opening. The DPM boundary condition type for the walls is trap, and the type for the sides along the X-axis and the tank opening is escape.

Geometry and grid generation is executed with a grid of the tetrahedral cells, based on the Gambit 2.4.6. The grid adopted in this paper is with 1352986 cells, based on the the grid sensitivity analysis. The minimum and maximum cell volumes in the domain are 4.448×10^{-6} m^3 and 2.342×10^{-3} m^3, respectively. The worst element is with a quality value of 0.76.

To analyse the droplet movement at different locations, the section above the opening is divided into 14 regions along the X-axis, and each interval width is 0.1 m, as shown in Fig. 1(b). The Z-axis is the centerline of the tank. The letters represent different region codes, and the numbers represent the coordinate values along the X-axis. The regions from A/A' to G/G' are increasing in distance from the centerline.

Airflow and Droplet

The droplet generation process from a tank can be described as follows: at the beginning, only water vapor is generated from the tank and comes into the ambient air in industrial production process. Then, the water vapor mixes with the ambient air and condenses to the droplets immediately due to heat transfer with the ambient air. After this phase transformation, a saturated airflow with many droplets is formed above the tank. When moving upward, the saturated moist airflow and droplets keep mixing with the

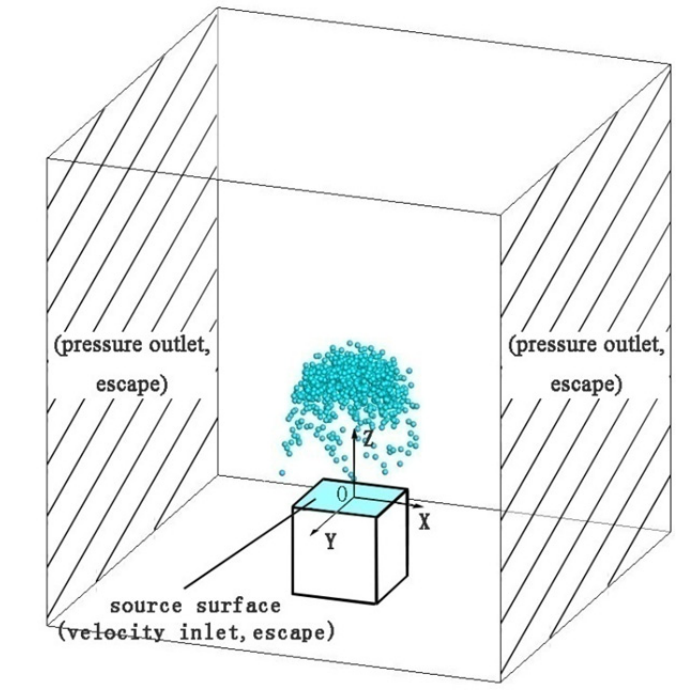

(a)

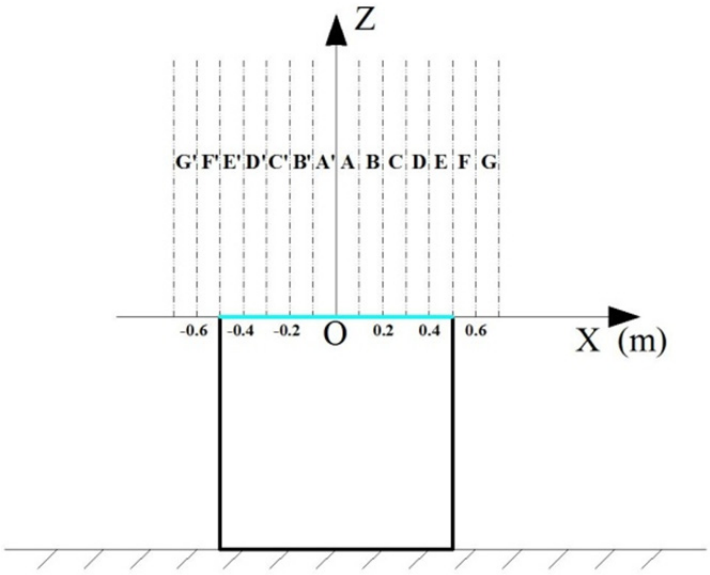

(b)

Fig. 1. Geometric schematic of droplets releasing from a tank in an industrial building (a) Geometric model; (b) The region schematic above the opening.

ambient air. The droplets begin to evaporate because the mix effect decreases the vapor concentration around the droplets. The objective of this paper is to investigate the evaporation and movement of the droplets after the droplet condensation, thus the simulation of the water condensation process is not discussed and the tank opening is simplified to be a boundary which releases the saturated moist air and droplets. The parameters influenced by water condensation, such as the initial diameter of droplets and the velocity of the saturated moist air, are based on previous researches (Xu, 2007; Zhang, 2010).

Air density is assumed to be constant for the reason that the density change of indoor air caused by the difference of water vapor content is less than 1% as there is no temperature difference. Governing equations for the gas phase are based on the continuity equation, N-S equations, energy equation and water vapor diffusion equation. It has been proved that k-ε turbulence models are suitable for predicting indoor air distribution (Chen, 1995; Round and Havet, 2002). Here, a realizable k-ε model is chosen, as turbulent viscosity and turbulent dissipation have been corrected in this model.

The initial droplet diameter adopted in this paper ranges from 1 μm to 50 μm based on a similar acidic droplet generation process from a pickling tank, in which the initial diameter of acidic droplets ranges from 0.1 μm to 50 μm (Zhang, 2010). A droplet population in one case corresponds to an identical initial diameter, D_i. The temperature distribution of a droplet can be treated as uniform when the Biot number of the droplet is less than 0.1 (Farid, 2003). $Bi = hD_d/\lambda < 0.1$, where h is the air heat transfer coefficient, λ is the thermal conductivity of the droplet, and D_d is the droplet diameter. Considering that the initial diameter has a range of 1 μm to 50 μm and λ is much larger than h, the droplet temperature T_d is assumed to be uniform. The Kelvin effect is neglected as the diameter is larger than 0.1 μm (Tang, 2000), so the water vapor partial pressure at the droplet surface is approximately equal to the water vapor pressure of the saturated air corresponding to the droplet temperature (Lian, 2006). Eq. (1) is used to calculate the water vapor partial pressure at the surface of a droplet, $P_{vap,d}$ (Kukkonen, 1989). A randomly walking model is used to describe the effect of airflow turbulence on the droplet trajectory.

$$P_{vap,d} = \exp[77.34 - (7235/T_d) - 8.2\ln T_d + 0.005711 T_d] \quad (1)$$

The evaporation rate of a droplet is calculated by Eq. (2) as follows:

$$N_i = k_c \left(\frac{P_{vap,d}}{RT_d} - \frac{P_{vap,\infty}}{RT_\infty} \right) \quad (2)$$

where N_i is mole flux of water vapor, kgmol m^{-2} s^{-1}; k_c is the mass transfer coefficient, m s^{-1}; the first term in brackets represents the water vapor concentration at the droplet surface, kgmol m^{-3}; the second term in brackets represents the water vapor concentration of the ambient air, kgmol m^{-3}. Because of evaporation, the droplet mass in the energy and momentum equations dynamically changes.

Heat exchange between droplets and air mainly includes convection heat transfer and evaporation, ignoring the radiation heat transfer. The energy equation of droplets is as follows:

$$m_d c_d \frac{dT_d}{dt} = hA_d (T_\infty - T_d) + \frac{dm_d}{dt} h_{fg} \quad (3)$$

where the left term represents the total enthalpy change of a droplet; the first term on the right represents the heat transfer by heat convection; the second term on the right represents the latent heat of vaporization.

The motion equation is represented as follows, according to Newton's second law:

$$m_d \frac{du_d}{dt} = V_d \frac{g(\rho_d - \rho)}{\rho_d} + F_{drag} + F_x \quad (4)$$

where the first term on the right represents the gravity and buoyancy; the second term on the right represents the drag force; the third term represents other external forces. The Brownian force and Saffman lift force are taken into consideration, ignoring the pressure gradient force, visual mass force and Basset force (Zhao *et al.*, 2004).

Solution Methods

A commercial software Fluent 6.3 is employed. A Lagrangian-Eulerian approach is adopted to solve the airflow (the continuous phase) and the droplets (the discrete phase). The droplets are injected into the domain after the continuous phase is converged.

The Continuous Phase

The SIMPLE algorithm is adopted to solve the pressure and velocity coupling (Montazeri *et al.*, 2015b). The pressure discretization scheme is PRESTO! while the discretization schemes for the convection terms and the viscous terms are the second-order upwind.

The Discrete Phase

Considering the interaction with the airflow, the droplet momentum, heat and mass transfer equations are solved in a two-way coupling method. The droplets time step tracks with the air flow time step. Trapezoidal and implicit schemes are used for high order scheme and the low order scheme in solving the equations of droplet motion, respectively (Fluent, 2006). A randomly walking model is used to describe the effect of airflow turbulence on the droplet trajectory.

Parameters

Three parameters are used to evaluate the evaporation and movement of the droplets, named $\overline{D_{dt}}$ (the mean diameter corresponding to the number of initial droplets), $\overline{D_d}$ (the mean diameter corresponding to the number of existing droplets), and $\overline{V_z}$ (the mean velocity along Z-axis corresponding to the number of existing droplets):

$$\overline{D_{dt}} = \frac{\sum_{j=1}^{n} D_j}{N_{di}} \quad (5)$$

where D_j represents the droplet diameter marked as j; N_{di} represents the initial droplet number, which is constant and equal to 808 in this paper.

$$\overline{D_d} = \frac{\sum_{j=1}^{n} D_j}{N_d} \quad (6)$$

where N_d represents the number of droplets actually existing at that moment, which is relevant to the case, time and selected region. The region which a droplet belongs to is determined by its coordinate value.

$$\overline{V_Z} = \frac{\sum_{j=1}^{n} V_{z\,j}}{N_d} \quad (7)$$

where V_{zj} represents the droplet velocity component in the positive direction of Z-axis.

When released in stagnant air, a particle will quickly reach its terminal settling velocity, V_{ter}. V_{ter} can be determined by the following equation (John and Spyros, 2006). It is an important parameter to present the droplet movement. For a evaporating droplet, V_{ter} decreases with the droplet diameter decreasing. This parameter is used to check the movement of droplet in the validation part.

$$V_{ter} = \left(\frac{4gD_d C_c \rho_d}{3C_D \rho} \right)^{1/2} \tag{8}$$

where C_c and C_D are the drag coefficients.

In fact, when a droplet is in airflow, V_{ter} could be used to present the velocity component difference along the gravity between the droplet and its surrounding air. This velocity difference is often called as the drift velocity (Sun, 2007). The mean terminal settling velocity $\overline{V_{ter}}$ of the droplets in this paper can be defined as the difference between $\overline{V_z}$ and the corresponding air velocity V_{gz}.

Cases

The cases in the numerical simulation are shown in Table 1. The initial number of the droplets is 808. The saturated moist air and the droplets from the opening is with an initial velocity of 0.3 m s^{-1} (Xu, 2007), and the direction is along the positive Z-axis. The initial temperature of the droplets and the saturated moist air flow is 30°C, which is identical to the indoor air. The droplets are released from the tank at t = 0 s in each case.

Simulation Validation

Inappropriate choices of governing equations and solvers may cause significant deviation in the simulation results (Li and Nielsen, 2011). The experimental study of the movement of free-fall evaporating droplets (T_d = 289 K, T_∞ = 293 K, RH = 70%) in humid, stagnant air by Hamey (1982) is used to verify the accuracy of the simulation results. Meanwhile, the terminal settling velocity V_{ter} is used to verify the accuracy of droplet movement. Solver settings in validation part are almost the same as the research cases. The differences between the validation study and research cases are the domain, grid, the boundary conditions and the injection type of the droplets. The comparison of the droplet diameters at the same drop height is shown in Figs. 2(a) and 2(b). The maximum deviations are 4.7% and 3.6% when D_i is 115 μm and 110 μm, respectively. The comparison of $\mathbf{V_{ter}}$ at the same droplet diameter is shown in Figs. 2(c) and 2(d). Both of the maximum deviations are 10.3% when D_i is 115 μm and 110 μm. The deviations may be caused by the boundary condition difference between the simulation and the experimental measurement, and the theoretical equation overlooks some forces acting on the droplet, such as Brownian force and the buoyancy.

RESULTS AND DISCUSSION

The Continuous Phase Characteristics

Fig. 3 shows the velocity component along Z-axis and relative humidity distribution of the continuous phase when the initial velocity of the saturated moist air is 0.3 m s^{-1} and the relative humidity of the ambient air is 50%. It presents that the saturated moist air generated from the tank forms a typical flow of a jet. After the saturated moist airflow releases from the tank opening, its fringe air begins to entrain and mix with the ambient air, and the air velocity and the vapor concentration of the fringe air decreases. With the continuous entrainment and mix effect, air velocity and the vapor concentration of the main air flow area decrease as well. In summary, after the saturated moist air comes into the ambient environment, it forms a nonuniform velocity and vapor concentration distribution. The vapor concentration and velocity in the regions close to the centerline of the tank are larger than those far away from the centerline.

It should be noted that although the droplets and the airflow are solved in a two-way coupling way method, the continuous phase change influenced by the evaporation and movement of droplets could be neglected according to the simulation results. That is because the droplets are released only once in a case, and the effect of their evaporation and movement on the continuous phase is limited. Thus, the continuous phase is considered to be constant in this paper.

Droplets Visualization

A droplet population with identical initial diameter forms a different diameter distribution after entering the indoor environment. Fig. 4 shows the droplet diameter changes in Case 3 and Case 4 after released from the tank (t = 0). Obviously, the droplet diameters decrease as time progresses because of evaporation. The diameters of the droplets far from the centerline of the tank change more quickly, and the droplets disappear earlier than the others. The droplet

Table 1. The simulation cases.

Case name	Initial diameter (μm) D_i	ARH and temperature	Initial velocity and temperature of the vapor moist air (m s^{-1})	Initial velocity and temperature of the droplets (m s^{-1})
Case1	1	50%/30°C	0.3 m s^{-1} 30°C	0.3 m s^{-1} 30°C
Case2	10	50%/30°C		
Case3	25	50%/30°C		
Case4	50	50%/30°C		
Case5	25	0%/30°C		
Case6	25	20%/30°C		
Case7	25	80%/30°C		

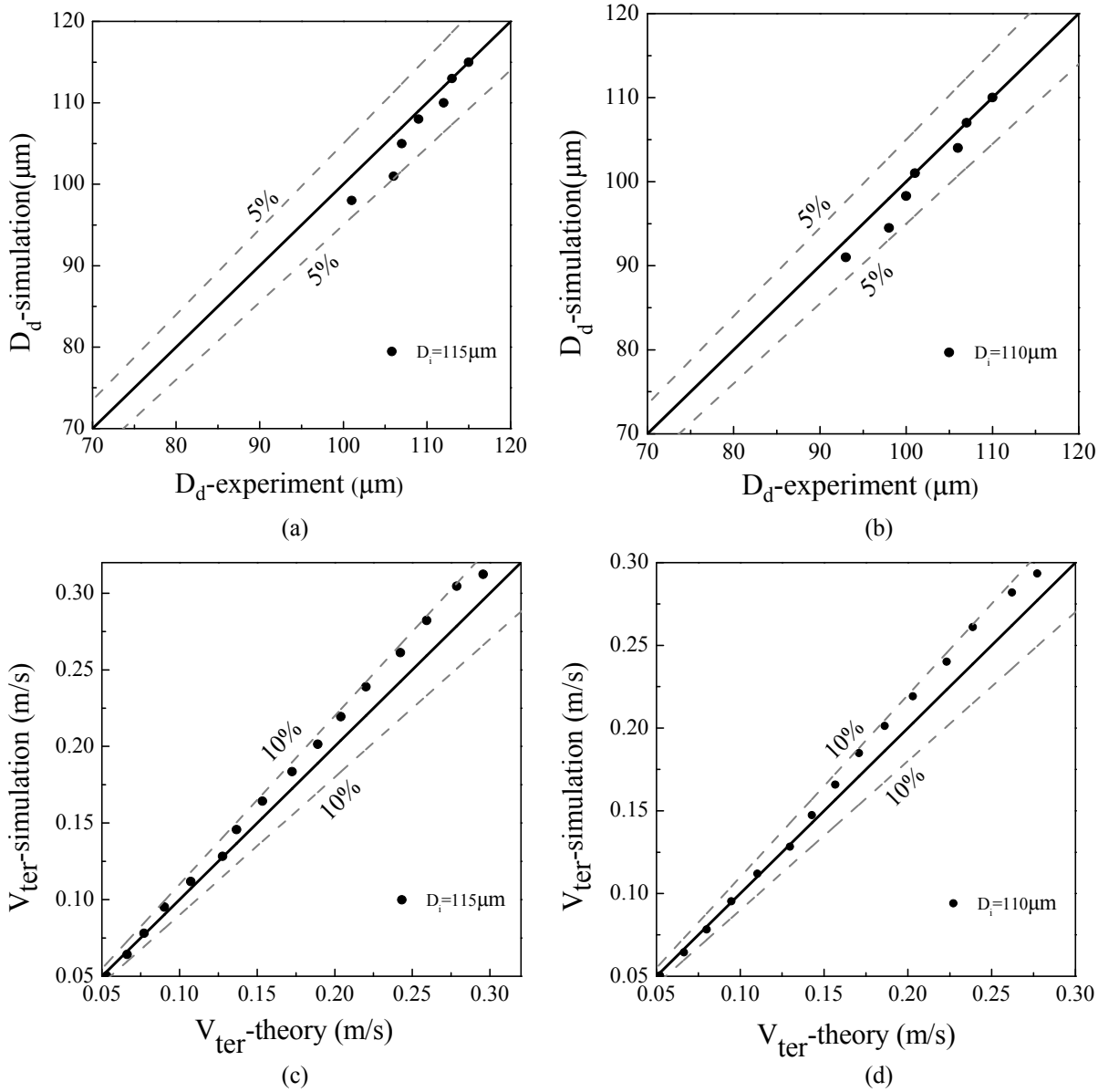

Fig. 2. Comparison of the experimental data and the simulation result (a) Comparison of D_d at the same drop height when D_i = 115 μm; (b) Comparison of D_d at the same drop height when D_i = 110 μm; (c) Comparison of v_{ter} at the same D_d when D_i = 115 μm; (d) Comparison of v_{ter} at the same D_d when D_i = 110 μm.

evaporation is relevant to the distance between the droplets and the centerline. Obviously, the droplets with an initial diameter of 25 μm change and disappear faster than those with an initial diameter of 50 μm.

Droplet Diameter Changes

The diameter evolution is strongly relevant to the distance between the droplets and the centerline. Fig. 5 quantitatively shows the mean diameter of the droplets, $\overline{D_d}$, in different regions along the X-axis in Case 4. The initial diameter is 50 μm, and the relative humidity of the ambient air is 50%. It only presents the $\overline{D_d}$ in the regions where the droplets exist. When t = 1 s, the size distribution is substantially uniform compared to the initial diameter. When t = 3 s, $\overline{D_d}$ decreases in all regions. $\overline{D_d}$ of the regions near the centerline are uniform, while $\overline{D_d}$ of the regions far from the centerline decrease sharply. When t = 8 s, the size continues to decease, and the mean diameter of the two regions nearest to the centerline is largest. When t = 12 s, the droplets in the regions far from the centerline disappear due to evaporation, and the existing droplets are mainly in the vicinity of the centerline. The symbol number shows a first increase and then decrease trend over time. The increase implies that the mix of air from the tank and the ambient environment makes the droplets diffuse to the regions far from the centerline. The decrease implies the evaporation makes the droplets far from the centerline totally evaporate quickly.

These results indicate that droplets in the regions near the centerline evaporate more slowly compared to droplets

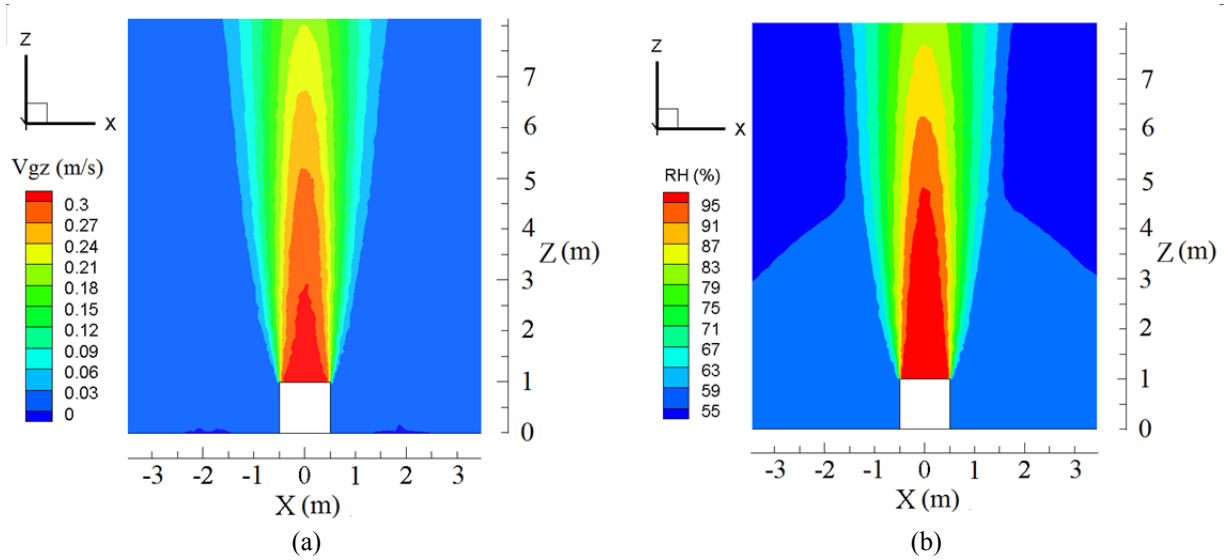

Fig. 3. The continuous phase parameter distribution when the ambient relative humidity is 50% (a) velocity component distribution along Z-axis; (b) relative humidity distribution.

farther from the centerline. This is mainly caused by the concentration difference of the vapor in the continuous phase. Although the air flow released with the droplets is saturated moist air, the vapor concentration of the air near the opening edge decreases sharply due to its entraining and mixing with the indoor air. Thus, the evaporation rate of droplets near the opening edge is fast because the vapor concentration difference increases between the droplet surface and the surrounding air, see Eq. (2). As time progresses, the entrainment and mix effect make the vapor concentration of the air near the centreline descend. The diameters of the droplets near the centerline begin to decrease as well. Meanwhile, it can be seen that the droplet size distribution is similar in the symmetric regions.

The number variation history of the droplets in different regions in Case 4 is shown in Fig. 6. The symmetric regions are merged for similar evaporation rates. For example, Region A and A' get merged into a large region. Due to the turbulent airflow, the number of droplets in each large region fluctuates, but the tendency of the number variation is quite obvious. Three typical variation tendencies are discussed. The droplets in Region A,A' are near the centerline, and the number decreases slowly because the vapor in Region A,A' keeps higher concentration. It seems that the saturated moist in Region A,A' protects the droplets from fast evaporation. The droplets in Region E,E' are near the opening edge, and the vapor concentration in these regions sharply decreases. Therefore, the droplets evaporate quickly, and their number almost decreases sharply with almost a linear variation. The number in Region F,F' first increases and then decreases. The increasing tendency occurs because the entrainment and mix effect of the air flow from the tank brings some droplets into the ambient air; the decreasing tendency is caused by evaporation.

Fig. 7 shows the dimensionless diameter $\overline{D_{dt}}/D_i$ change history of the droplets when the relative humidity of the ambient air is 50%. $\overline{D_{dt}}$ is the mean diameter of the entire droplet population, which represents the evaporation rate of the entire population. The evaporation time of all of the droplets increases when the initial diameter increases. When D_i = 1 μm, $\overline{D_{dt}}/D_i$ becomes 0 in no more than 0.5 s with a very fast decrease in size. When D_i = 10 μm, 25 μm and 50 μm, the evaporation time is 2.8 s, 6.9 s and 17.2 s, respectively.

The variation tendency of $\overline{D_{dt}}/D_i$ could be divided into three stages when the initial diameter is larger than 10 μm. When the droplets initially leave the tank, the variation of $\overline{D_{dt}}/D_i$ slightly decreases. Then, $\overline{D_{dt}}/D_i$ decreases linearly. When nearly all of the droplets have evaporated, the decrease rate of $\overline{D_{dt}}/D_i$ slows down. The third diameter variation tendency is because the droplets far from the centerline are totally evaporated and the droplet evaporation near the centerline is restrained by the higher vapor concentration. This diameter evolution is quite different from that when a droplet is in a uniform airflow (Sun and Ji, 2007; Xie *et al.*, 2007). In their researches, a droplet diameter change rate when it nearly totally evaporates could be very fast.

Movement of the Droplets

Fig. 8 shows $\overline{V_z}$ changes over time in Case 4, where $\overline{V_z}$ represents the mean velocity component in the Z-axis of the droplets in different regions. As time passes, $\overline{V_z}$ in each region increases. $\overline{V_z}$ in the regions near the centerline is larger than that farther from the centerline. Fig. 8 also shows the air velocity in Plane XOY, V_{gz}, corresponding to a Z-axis value equal to the mean height of all of the droplets at different times. V_{gz} near the centerline decreases, but it increases far from the centerline over time. $\overline{V_z}$ approaches to V_{gz} over time.

The distribution of $\overline{V_z}$ over time in Fig. 8 is because $\overline{V_{ter}}$ turns small. When the mean droplet diameter $\overline{D_d}$ turns small, $\overline{V_{ter}}$ decreases. Thus, $\overline{V_z}$ in each region increases over time. Likewise, $\overline{V_z}$ far from the centerline

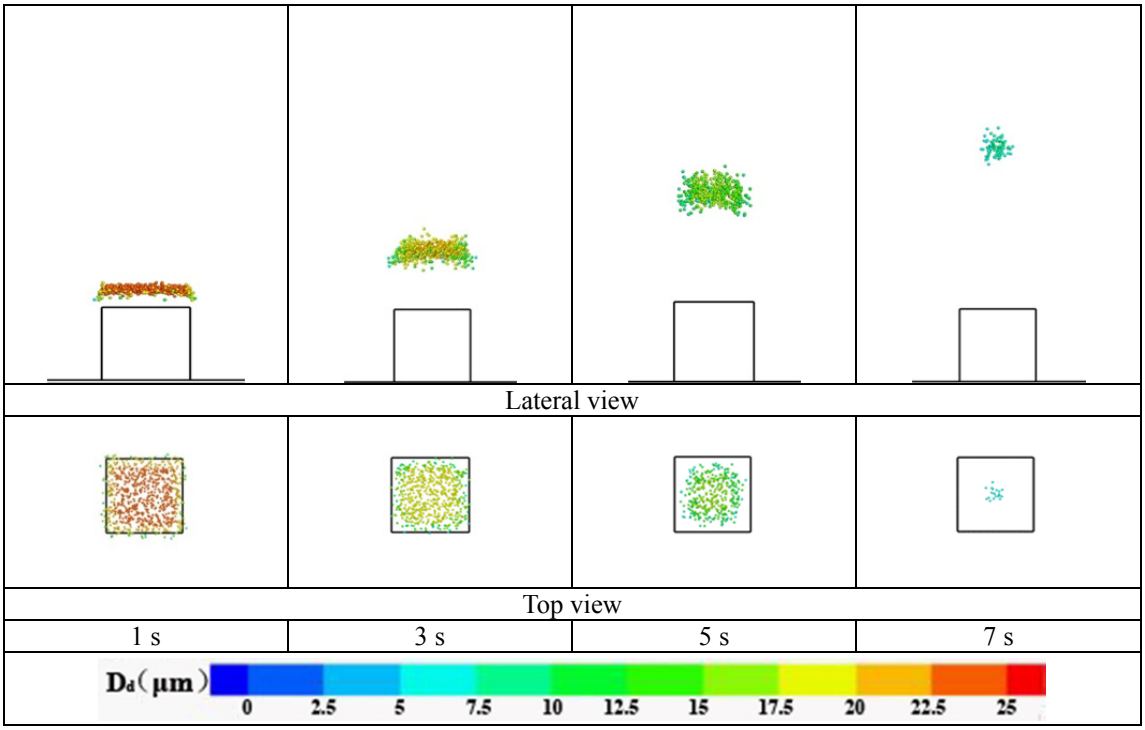

(a)

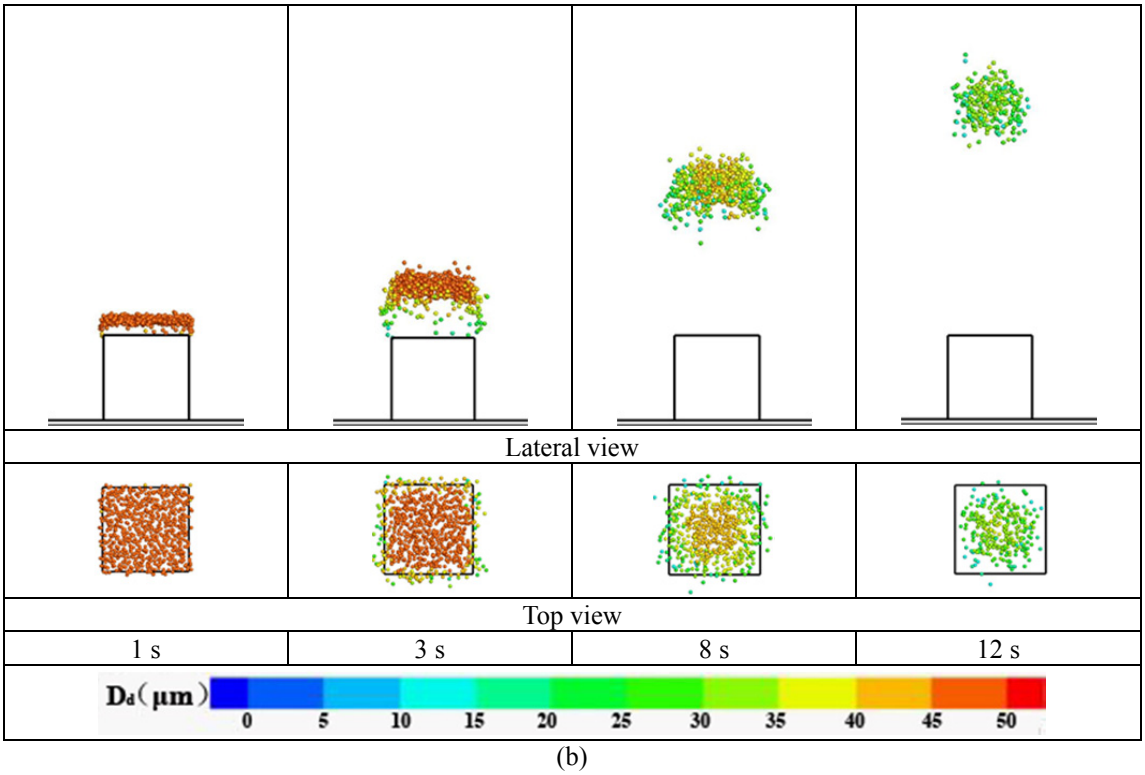

(b)

Fig. 4. Schematic diagram of the droplet diameter change history (a) D_i = 25 μm in Case 3; (b) D_i = 50 μm in Case 4.

is closer to the corresponding V_{gz} over time because the droplets far from the centerline evaporate faster, and $\overline{V}_{ter}$ turns more small. These results reveal that the droplets with identical initial velocity formed uniform velocity distributions over time.

$\overline{V}_z$ of the entire droplet population over time after the droplets injected to the domain 0.1 s are shown in Fig. 9, where the relative humidity of the ambient air is 50%. V_z at 0.1 s is lower than the initial droplet velocity 0.3 m s^{-1} in all three cases because the droplets quickly reaches their drift velocity. When D_i are 25 μm and 50 μm, the curves present a first decrease and then increase tendency. After

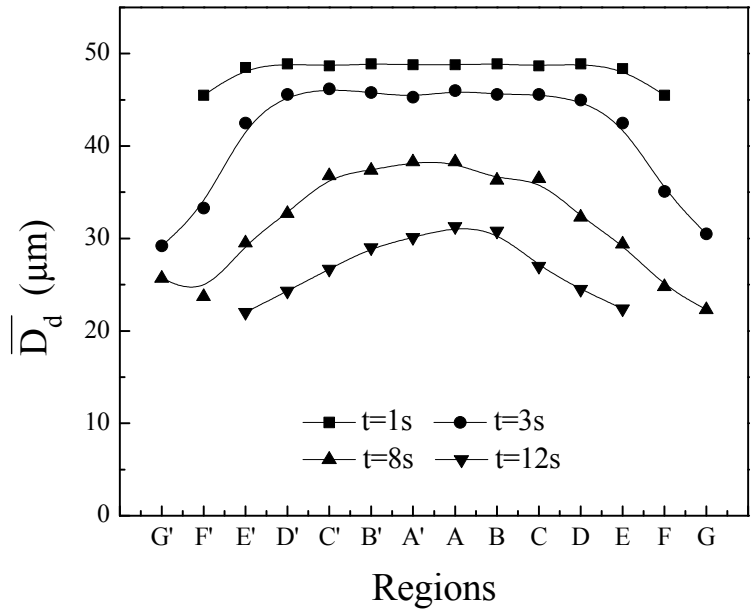

Fig. 5 . The distribution of $\overline{D_d}$ in different regions at D_i = 50 μm.

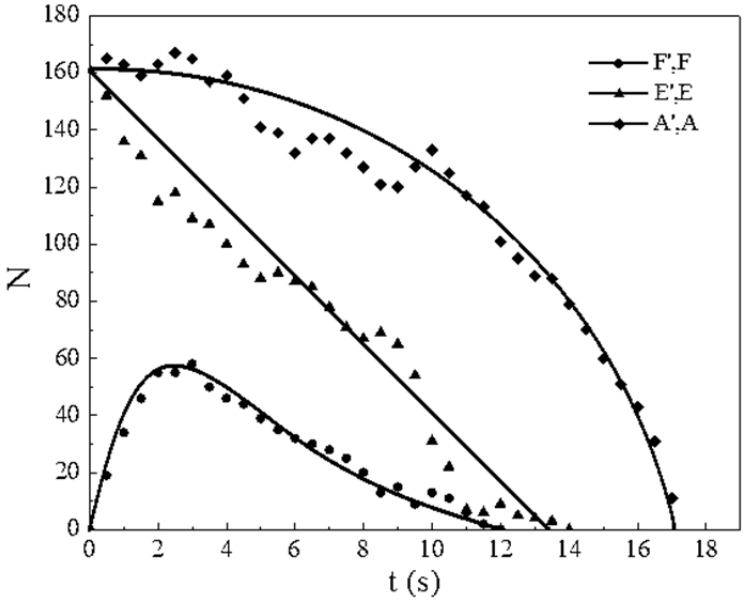

Fig. 6. The number variation history of the droplets in different regions in Case 4.

the droplets come into the domain, the mix and entrainment of airflow make some droplets gradually move into the regions where the airflow velocity is smaller, as seen the droplet number variation in Region F,F' of Fig. 6. The lower airflow speed makes the velocity of the droplets coming into these regions get small. Thus at the beginning, $\overline{V_z}$ shows a decreasing tendency. With the time progressing, $\overline{V_z}$ increases in all three cases. The reason for this is that the evaporation makes the droplet diameters decrease, resulting in the terminal settling velocity decreasing. The minimum $\overline{V_z}$ appears at t = 1 s and t = 2.6 s when D_i = 25 μm and 50 μm, respectively. However, when D_i is 10 μm, the curve only shows an increase trend over time. The reason why the decrease trend do not appear may be that the droplets with D_i = 10 μm totally evaporate quickly, and the droplets in low velocity regions hardly exist.

The three curves from Fig. 9 indicates $\overline{V_z}$ with a larger initial diameter is apparently smaller than that with a smaller initial diameter. That is because a larger initial diameter results in a larger terminal settling velocity, which makes the velocity difference between a droplet and its surrounding air larger.

The Influence of ARH

The relative humidity of the ambient air (ARH) has a significant effect on droplet evaporation, according to Sun and Ji's (Sun and Ji, 2007) and Xie's study (Xie *et al.*, 2007). For the droplets generated from the tank, surprisedly,

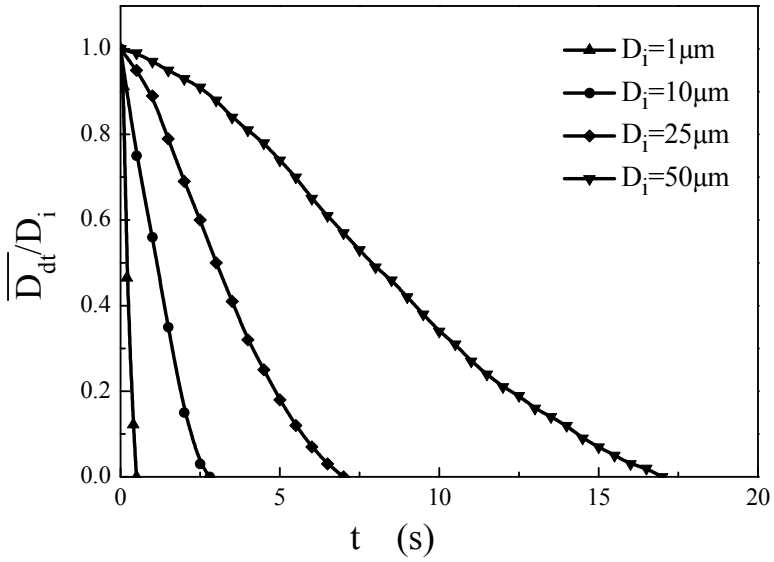

Fig. 7. The dimensionless diameter $\overline{D_{dt}} / D_i$ change history of the droplets when ARH is 50%.

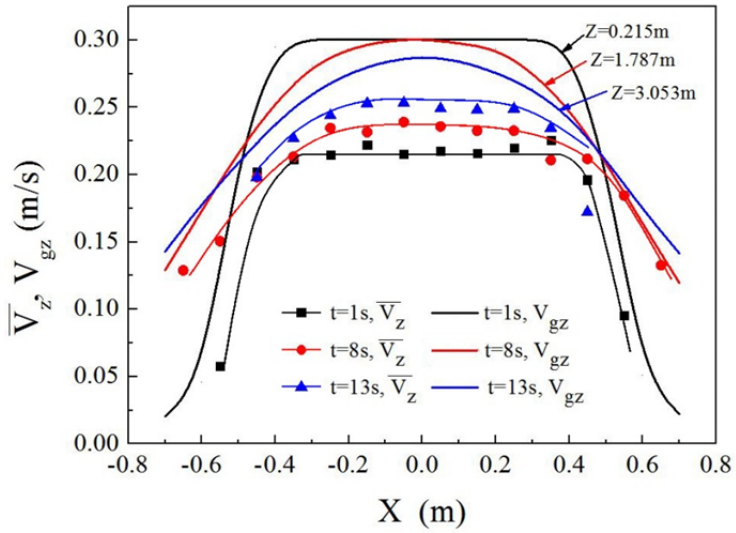

Fig. 8. $\overline{V_z}$ of droplets in different regions and V_{gz} changes over time in Case 4.

ARH has a rather limited effect on the evaporation and movement of the droplet population.

Fig. 10 shows the effect of ARH on $\overline{D_{dt}}$ when D_i = 25 μm. $\overline{D_{dt}}$ change decreases and the evaporation time is prolonged as ARH increases. The evaporation time shows a range of 6.3 s to7.2 s when ARH changes from 20% to 80%, but the difference is no more than 1 s. Furthermore, the $\overline{D_{dt}}$ difference is no more than 5 μm at the same time in these cases. The small differences can be explained that although the relative humidity of the ambient air changes from 20% to 80%, the relative humidity of the air where the main droplets stay does not vary greatly as the air flow released from the tank is saturated. The difference of the evaporation time caused by ARH variation is almost 1/17 of that caused by the initial diameter variation. The small difference in the evaporation time and $\overline{D_{dt}}$ at different ARH values reveals that droplet evaporation is not very sensitive to ARH.

Evaporation causes the droplet population to reach a different maximum height H in different conditions. Fig. 11 shows the maximum attainable height of the droplet population at different initial diameters (on the left Y-axis) and ambient relative humilities (on the right Y-axis). The difference of H caused by ARH variation is almost 1/10 of that caused by the initial diameter variation. When the initial diameter changes from 1 μm to 50 μm at ARH is equal to 50%, the maximum height shows an approximately linear variation, and H ranges from 0.15 m to 4 m. When ARH varies from 0 to 80% at D_i = 25 μm, H ranges from 1.75 m to 2.15 m. The small differences could be explained that the droplet change is not large with ARH changing.

The results from Figs. 10 and 11 reveal that the evaporation and motion of the droplets from the tank are not very sensitive to the relative humidity of the ambient

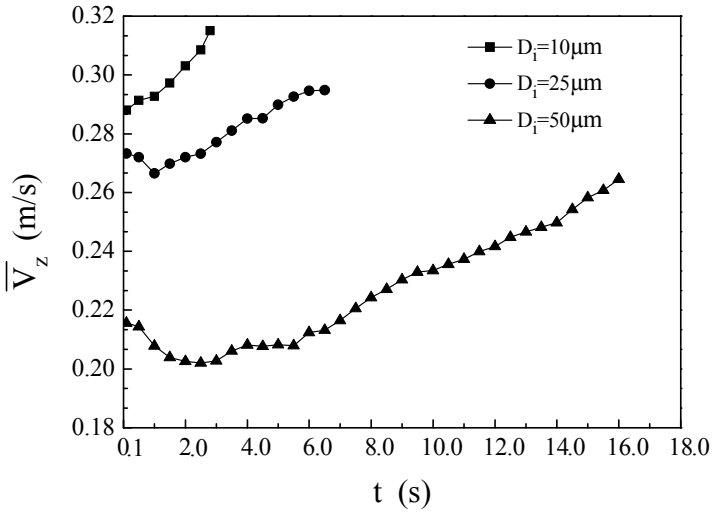

Fig . 9. $\overline{V_z}$ of the entire droplet population over time.

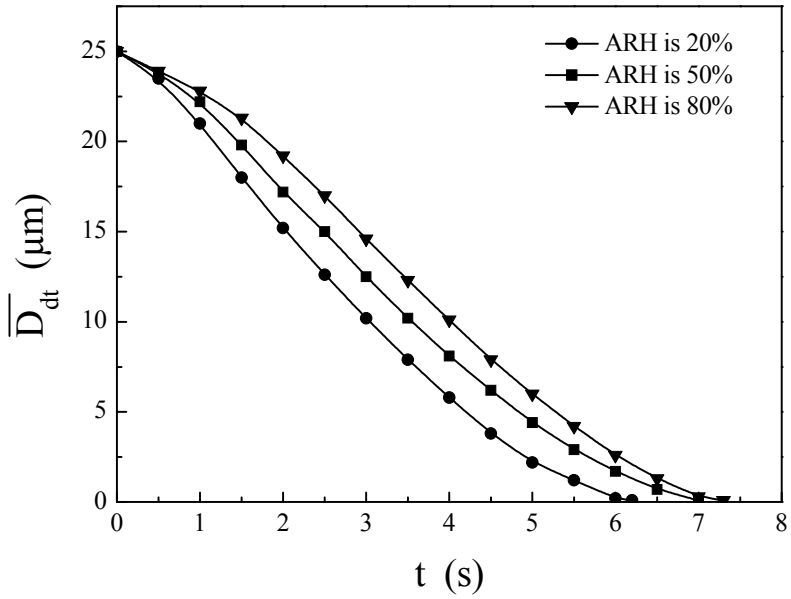

Fig. 10. $\overline{D_{dt}}$ evolution at different ARH.

air from the pressure outlet boundaries. Its effect on the droplet movement could be neglected in ventilation design.

CONCLUSIONS

A droplet-air two phase flow was studied in this paper. The droplets were with a uniform initial diameter distribution, and the airflow was with a nonuniform distribution. The evaporation and movement of the droplets were discussed and the scientific reasons were analyzed. The results are intended to provide a reference for reasonable and effective ventilation methods of droplet control. The main conclusions are as follows:

1. Compared to droplet evaporation in a uniform vapor concentration environment, the evaporation of droplets in a nonuniform vapor concentration environment depends on their locations. The droplets closer to the centerline of the tank show a slower diameter decrease and have a longer evaporation time. When the relative humidity of the ambient air is 50%, the evaporation time of the droplet population less than 1 μm is less than 0.5 s, while the evaporation time ranges from 2.8 s to 17.2 s when the initial diameter varies from 10 μm to 50 μm.

2. The combination of droplet diameter distribution and the air flow velocity distribution around the droplets causes the velocity difference of the droplets. The droplet diameter difference makes the velocity difference between the droplets and their surrounding air near the centerline larger than that far from the centerline. The air flow makes the velocity of the droplets closer to the centerline larger as well. Thus, the velocity difference of droplets in different regions should be taken into consideration in ventilation on droplet control.

3. Surprisedly, the relative humidity of the ambient air has a rather limited effect on the evaporation and movement

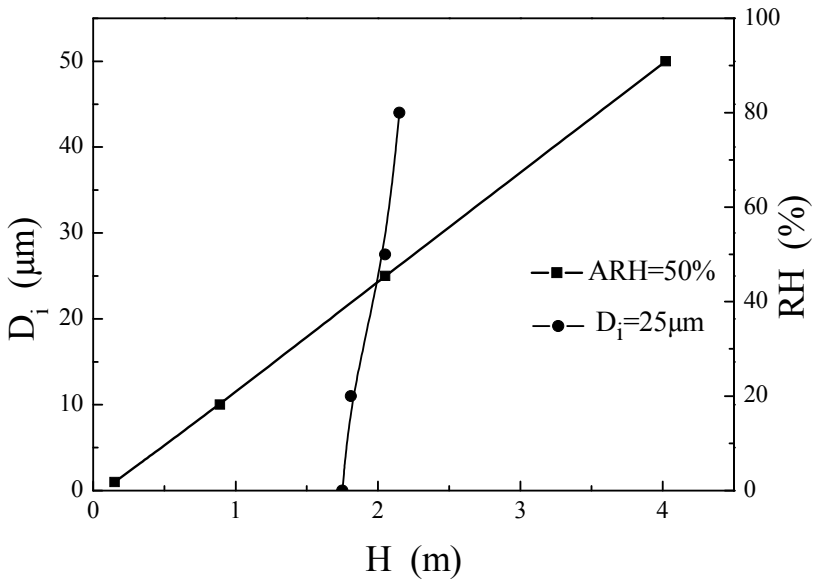

Fig. 11. The maximum height of the droplets in different cases

of droplets, compared to that of the initial diameter. Its effects (varying from 20% to 80%) on the evaporation time variation and the terminal height variation are merely about 1/17 and 1/10 of the effects caused by the initial diameter variation (1 μm–50 μm), respectively. Thus, the effect of the relative humidity of the ambient air on droplet control could be neglected in ventilation.

ACKNOWLEDGEMENT

This research was supported by the Key Project of the National Natural Science Foundation of China (No. 51238010) and the National Science Fund for Distinguished Young Scholars of China (No.51425803)

REFERENCES

Achenbach, P.R. and Trechsel, H.R. (1982). Evaluation of Current Guidelines of Good Practice for Condensation Control in Insulated Building Envelopes, Thermal Performance of the Exterior Envelopes of Buildings. Proceedings of ASHRAE/DOE Conference, Las Vegas, USA, 1982, ASHRAE, Atlanta, pp. 1090–1107.

Allen, M.D. and Raabe, O.G. (1982). Reevaluation of Millikan's Oil Drop Data for the Motion of Small Particles in Air. *J. Aerosol Sci*. 13: 537–547.

ASHRAE (2007). *2007 HVAC Applications*. American Society of Heating, Refrigeration and Air-Conditioning Engineers, Atlanta.

Chen, Q. (1995). Comparison of Different k-ε Models for Indoor Air Flow Computations. *Numer. Heat Transfer, Part B* 28: 353–369.

Cheong, H.W. (1986). A Receding Interface Model for the Drying of Slurry Droplets. *AlChE J.* 32: 1334–1346.

Dufour, L. and Defay, R. (1963). *Thermodynamics of Clouds*. Academic Press, New York and London.

Farid, M. (2003). A New Approach to Modelling of Single Droplet Drying. *Chem. Eng. Sci*. 58: 2985–2993.

Hamey, P.Y. (1982). The Evaporation of Airborne Droplets. MSc Thesis, Granfield Institute of Technology, Bedfordshire, UK, pp. 48–58.

Hyunhee, P., Jang, J.K. and Shin, J.A. (2011). Quantitative Exposure Assessment of Various Chemical Substances in a Wafer Fabrication Industry Facility. *Saf. Health Work* 2: 39–47.

John, H.S and Spyros, N.P (2006). *Atmospheric Chemistry and Physics*. John Wiley & Sons, Inc. Hoboken.

Kadja, M. and Bergeles, G. (2003). Modelling of Slurry Droplet Drying. *Appl. Therm. Eng*. 23: 829–844.

Kim, H., Jeon, S., Song, M. and Kim, K. (2014). Numerical Simulations of Water Droplet Dynamics in Hydrogen Fuel Cell Gas Channel. *J. Power Sources*. 246:679–695.

Kukkonen, J., VESALA, T. and Kulmala, M. (1989). The Interdependence of Evaporation and Settling for Airborne Freely Falling Droplets. *J. Aerosol Sci.* 20: 749–763.

Li, J. and Zhou, Y. (2015). Occupational Hazards Control of Hazardous Substances in Clean Room of Semiconductor Manufacturing Plant Using CFD Analysis. *Toxicol. Ind. Health* 31: 123–139.

Li, Y. and Nielsen, P.V. (2011). CFD and Ventilation Research. *Indoor Air* 21: 442–453.

Lian, Z. (2006). *Heat and Mass Transfer: Fundamentals and Equipment*. China Building Industry Press, Beijing.

Liu, L. (2011). Expiratory Droplet Exposure between Individuals in a Ventilated Room. Ph.D. Thesis. The University of Hong Kong, Hong Kong.

Miller, R.S., Harstad, K.J. and Bellan, J. (1998). Evaluation of Equilibrium and Non-equilibrium Evaporation Models for Many-droplet Gas-liquid Flow Simulations. *Int. J. Multiphase Flow* 24: 1025–1055.

Montazeri, H., Blockena, B. and Hensena, L.M.J. (2015a). Evaporative Cooling by Water Spray Systems: CFD Simulation, Experimental Validation and Sensitivity Analysis. *Build. Environ*. 83: 129–141.

Montazeri, H., Blockena, B. and Hensena, L.M.J. (2015b). CFD Analysis of the Impact of Physical Parameters on Evaporative Cooling by a Mist Spray System. *Appl. Therm. Eng*. 75: 608–622.

Pruppacher, R.H. and Klett, D.J. (2004). *Microphysics of Clouds and Precipitation*, Kluwer academic Publishers, Dordrecht.

Round, O. and Havet, M. (2002). Computation of the Airflow in a Pilot Scale Clean Room Using k-ε Turbulence Models. *Int. J. Refrig*. 25: 351–361.

Sazhin, S.S. (2006). Advanced Models of Fuel Droplet Heating and Evaporation. *Prog. Energy Combust. Sci.* 32: 162–214.

Schlottke, J. and Weigand, B. (2008). Direct Numerical Simulation of Evaporating Droplets. *J. Comput. Phys.* 227: 5215–5273.

Shanthanu, S., Raghuram, S. and Raghavan, V. (2013). Transient Evaporation of Moving Water Droplets in Steam–hydrogen–air Environment. *Int. J. Heat Mass Transfer* 64: 536–546.

Sirignano, A.W. (2000) *Fluid Dynamics and Transport of Droplets and Sprays*. Cambridge University Press, New York.

Sun, W. (2007). Transport of Droplets with Contaminant is Air-conditioned Room and Thermal Calculation of Buildings. Ph.D. Thesis. University of Science and Technology of China.

Sun, W. and Ji, J. (2007). Transport of Droplets Expelled by Coughing in Ventilated Rooms. *Indoor Built Environ.* 16: 493–504.

Sun, Y. (1997). *Concise Ventilation Design Manual*. China Building Industry Press, Beijing.

Tang, N.T. (1999). In *Aerosol Chemical Processes in the Environment*, Chapter 4, Spurny, R.K. (Ed.), CRC Press, Boca Raton, p. 67.

Varghese, S. and Gangamma, S. (2007). Evaporation of Water Droplets by Radiation: Effect of Absorbing Inclusions. *Aerosol Air Qual. Res*. 7: 95–105.

Xie, X., Li, Y., Chwang, A.T.Y., Ho, P.L. and Seto, W.H. (2007). How Far Droplets Can Move in Indoor Environments – Revisiting the Wells Evaporation-Falling Curve. *Indoor Air* 17: 211–225.

Xu, J. (2007). *Machine Design Manual of Heating Ventilation and Air-conditioning*. Tongji University Press, Shanghai.

Zhang, Q. (2010). Research of Plain Carbon Steel Pickling Acid-mist Dressing. MSc Thesis. Northeastern University, Shenyang.

Zhao, B., Zhang, Y., Li, X., Yang, X. and Huang, D. (2004). Comparison of Indoor Aerosol Particle and Deposition in Different Ventilated Rooms by Numerical Method. *Build. Environ.* 39:1–8.

Zhou, Z., Wang, G., Chen, B., Guo, L. and Wang, Y. (2013). Evaluation of Evaporation Models for Single Moving Droplet with a High Evaporation Rate. *Powder Technol.* 240: 95–102.

Zhu, X., Liao, Q., Sui, P.C. and Djilali, N. (2010). Numerical Investigation of Water Droplet Dynamics in a Low-temperature Fuel Cell Microchannel: Effect of Channel Geometry. *J. Power Sources*. 195: 801–812.

Received for review, March 28, 2015
Revised, June 25, 2015
Accepted, August 4, 2015